Chemistry at and near the Surface of Liquid Sulfuric Acid: A Kinetic, Thermodynamic, and Mechanistic Analysis of Heterogeneous Reactions of Acetone

Joanna L. Duncan, Liesl R. Schindler, and Jeffrey T. Roberts*

Department of Chemistry, University of Minnesota, Minneapolis, Minnesota 55455-0431

Received: April 22, 1999; In Final Form: June 23, 1999

The interactions of gas-phase acetone with liquid sulfuric acid solutions are described. The solutions were prepared as 0.05−0.10 μm thick films deposited on single-crystal metal substrates. Experiments were carried out over broad ranges of acid composition (70 − >96 wt % H_2SO_4), temperature (180−220 K), and acetone pressure (10^{-7}−10^{-3} Pa). Two types of measurements are reported: the time-dependent acetone uptake probability, and the infrared spectra of absorbed acetone and its reaction products. From the infrared measurements, a reaction scheme is identified in which gas-phase acetone is taken up by sulfuric acid to form protonated acetone. In solutions containing more than 70 wt % H_2SO_4, protonated acetone undergoes a self-condensation/dehydration reaction to form mesityl oxide. In films that contain 85 wt % or more H_2SO_4, a second reaction sequence occurs, ultimately resulting in the formation of trimethylbenzene. The uptake probability measurements are consistent with the infrared data. In 70 wt % H_2SO_4, the acetone uptake probability rapidly decreases from an initial value near unity to a steady-state value of zero, due to the formation of a saturated acetone + sulfuric acid solution. The Henry's law solubility constants of acetone in 70 wt % H_2SO_4 were obtained from the integrated uptake measurements. The temperature dependence of the measurements implies that the standard-state enthalpy and entropy changes of acetone solution in 70 wt % sulfuric acid are −66 kJ mol^{-1} and −249 J mol^{-1} K^{-1}, respectively. In the more concentrated films, the steady-state uptake probability is never measured to be zero, since absorbed acetone goes on to form the condensation/dehydration products. A two-step kinetic scheme is proposed to account for the reactions of acetone in sulfuric acid. By fitting the data to the model predictions, the Henry's law solubility constants and the reaction rate constants may be estimated.

Introduction

The past several years have witnessed an explosion of interest in reactions that occur at or near the liquid−vapor interface.[1−3] The liquid−vapor interface is ubiquitous in the natural environment, most obviously in marine and other aquatic regions, but also in the atmosphere, where large numbers of liquid aerosol particles are present.[4] From the perspective of fundamental science, liquid surface chemistry is interesting because of the extraordinarily broad range of phenomena that are involved in liquid surface-mediated transformations of gas-phase reactants into gas- or condensed-phase products, for instance adsorption and desorption, surface reactivity, transport between surface and bulk, and bulk-phase diffusion and reactivity. Many of these phenomena are also encountered in other classes of interfacial reactions, but some are unique or nearly unique to liquid interfaces. For example, Davidovits and co-workers have proposed a mechanism for surface-to-bulk transport in which the slow step for transport is formation of a critical-sized cluster of an adsorbed molecule and the molecules that make up the liquid.[5] Such a mechanism would be inoperative for most solids, which have considerably more rigid lattices.

The challenges presented by the liquid−vapor interface are of an experimental as well as a conceptual nature. Some of these challenges are a consequence of the relatively high vapor pressures of many liquids. The majority of surface-sensitive investigative methods operate best under high-vacuum conditions, and many studies of the liquid−vapor interface have therefore been restricted to low vapor pressure liquids.[6−10] This situation has changed considerably with the development of nonlinear optical probes such as second harmonic generation (SHG) and sum frequency generation (SFG),[11−13] but these experiments have the disadvantage of being difficult to implement and interpret. Moreover, SHG and SFG are insensitive to bulk chemistry, and so may provide an incomplete mechanistic picture of some liquid surface-mediated processes.

There is an ever expanding literature on the structural and dynamical properties of the liquid sulfuric acid surface. Particularly noteworthy in this regard are the SFG studies of Schultz et al.[14,15] and the molecular beam scattering work of Nathanson and co-workers.[16−18] The SFG studies have focused on the characterization of non-hydrogen bonded OH groups at the sulfuric acid surface and on the identification of adsorbed HCl. Due to the highly associated nature of sulfuric acid, the coverage of "free" surface OH groups is a sensitive function of acid composition, and in fact no non-hydrogen bonded OH groups have been observed by SFG for solutions containing more than ∼5 wt % H_2SO_4. Molecular beam studies have explored the scattering of numerous substances from the surface of the H_2O + H_2SO_4 azeotrope and from the surfaces of nonazeotropic, supercooled H_2O + H_2SO_4 solutions.[19] Among the substances investigated in these studies are the organic compounds ethanol, dimethyl ether, acetaldehyde, and propene.

Numerous researchers have investigated the kinetics of gas uptake by liquid sulfuric acid. These studies have been motivated by a desire to characterize the interactions of atmospherically abundant compounds with laboratory surrogates for tropospheric

* Corresponding author.

10.1021/jp991322w CCC: $18.00
Published on Web 08/07/1999

and stratospheric cloud particles. Many reports have appeared on the uptake of inorganic compounds by sulfuric acid; compounds studied include $ClONO_2$, N_2O_5, HO_2NO_2, HONO, HCl, HBr, and SO_2.[20−31] There is a comparative dearth of work on the uptake of organic substances, and most of it has concerned formaldehyde (H_2CO). Jayne et al. measured H_2CO mass accommodation coefficients by $H_2O + H_2SO_4$ over broad concentration ranges and at temperatures between 230 and 298 K.[32] They concluded that physical uptake dominates in mildly acidic solutions (less than ∼60 wt % H_2SO_4), that formaldehyde dissolves to form the protonated species H_2COH^+ in more concentrated solutions, and that a limited amount of the hydrolysis product $CH_2(OH)_2$ forms at all concentrations. Tolbert and co-workers studied formaldehyde uptake by 60−75 wt % H_2SO_4 between 208 and 233 K.[33] Under these conditions, uptake was irreversible. In more recent work, Iraci and Tolbert used infrared spectroscopy to identify a formaldehyde polymer as the principal uptake product.[34] No evidence was obtained for protonated formaldehyde, but the temperature range investigated (197−215 K) was well below that studied by Jayne. On the basis of the Henry's law solubilities, Iraci and Tolbert concluded that $H_2O + H_2SO_4$ particles are not a significant sink for formaldehyde in the troposphere.

We have developed an alternative approach to the study of the sulfuric acid surface.[35−37] It involves the deposition of ultrathin, liquid sulfuric acid films onto single-crystal metal substrates. Film composition can be varied over a broad range, from the $H_2O + H_2SO_4$ azeotrope, which contains ∼96 wt % H_2SO_4, to solutions of composition 60 wt % H_2SO_4. Because the films are ultrathin (typically ∼100 molecular layers thick), they have very high surface area-to-volume ratios. For this reason, one can employ spectroscopic methods that are inherently bulk-sensitive (e.g., infrared spectroscopy) to interrogate the adsorbed and bulk phases simultaneously. The properties of the films are otherwise indistinguishable from those of bulk sulfuric acid samples. The films, which are at equilibrium with the vapor phase, are extraordinarily stable with respect to H_2SO_4 evaporation. This is a consequence of the fact that the equilibrium vapor phase over a sulfuric acid solution consists almost entirely of H_2O. If the H_2O partial pressure over a film is held constant, then so are film composition and thickness.

Recently, we published preliminary results of a study of the interaction of acetone [$(CH_3)_2CO$] with sulfuric acid.[37] In that work, Fourier transform infrared reflection absorption spectroscopy (FTIRAS) was used to establish the heterogeneous reaction pathway shown in Scheme 1. To summarize, gas-phase acetone (**1**) is taken up by sulfuric acid to form protonated acetone (**2**). In acids of composition ≤70 wt % H_2SO_4, **2** is the sole observed uptake product. In more concentrated acids, a series of reactions occurs, beginning with the condensation of two equivalents of **2** to form protonated mesityl oxide (**3**). Mesityl oxide formation presumably occurs via a two-step sequence, first the aldol condensation of two protonated acetone molecules, and then the dehydration of the resulting product. In acids containing 75−85 wt % H_2SO_4, no further reactions occur, but in the ≥ 85 wt % acid, an additional condensation/dehydration sequence takes place, resulting in the formation of trimethylbenzene (**4**). The conversion of acetone to trimethylbenzene had been identified before, but only in room-temperature solutions of acetone and concentrated (∼96 wt %) sulfuric acid. The significance of the work was therefore 2-fold: it showed that acetone reacts in <96 wt % sulfuric acid, and it established that the reaction occurs via accommodation of acetone from the gas phase.

SCHEME 1: Pathway for the Conversion of Three Equivalents of Acetone to One Equivalent of Trimethylbenzene

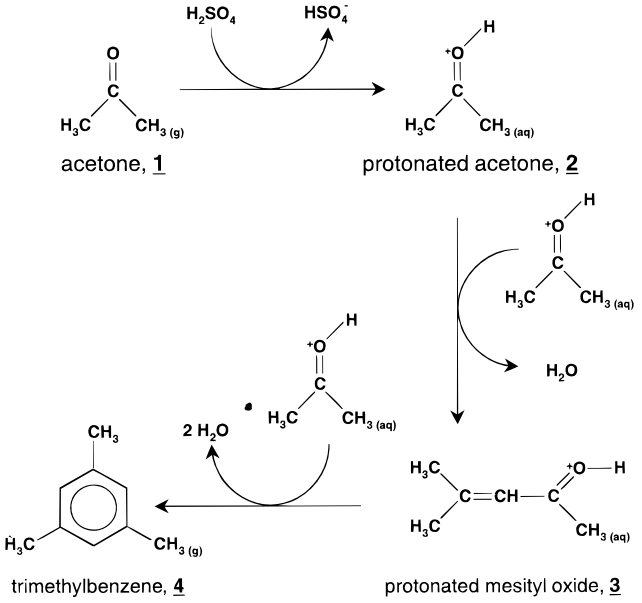

In this work, we expand on our earlier study of the acetone + sulfuric acid system. In particular, we consider the kinetics of acetone uptake, and we analyze the uptake thermodynamics and kinetics as a function of sulfuric acid composition and temperature. We also present additional FTIRAS data on the mechanism of the acetone-to-trimethylbenzene reaction. We conclude with a discussion of the significance of these results for the chemistry of the remote upper troposphere.

Experimental Section

The experiments were carried out in two vacuum chambers described in detail elsewhere.[35] Both of the vacuum chambers were constructed of suitably modified, 10-in. diameter, stainless steel bell jars. The chambers were pumped continuously by ion getter pumps and intermittently by titanium sublimation pumps. Their base pressures were $\sim 10^{-8}$ Pa, but during experiments they operated at total pressures between 10^{-8} and 10^{-3} Pa. One of the vacuum chambers was designed for high-quality temperature-programmed desorption (TPD) and gas uptake measurements. In the context of the work described in this paper, the most important piece of instrumentation on that chamber was a computer-interfaced quadrupole mass spectrometer of mass range 1−400 amu. The other vacuum chamber was designed and used primarily for FTIRAS. Infrared radiation was transmitted in and out of the vacuum chamber via calcium fluoride windows, and it was detected with a standard MCT/A detector. The reflection angle was 4° with respect to the sample plane. Most of the infrared data were collected between 1000 and 4000 cm^{-1}, the low-frequency cutoff being determined by the choice of CaF_2 as the material for the transmission windows. The spectra were acquired using 32 scans at a resolution of 4 cm^{-1} with an average data point spacing of 1.95 cm^{-1}. The FTIRAS chamber was also equipped with a quadrupole mass spectrometer, which was used to monitor gas-phase composition and dose purity.

The reaction vessels were outfitted with sample manipulators capable of rotation, as well as translation along three mutually orthogonal axes. A single crystal, either 111-oriented Pt or 100-

oriented W, was mounted on each of the manipulators. The single crystals served as substrates for the sulfuric acid films, the preparation and characterization of which are described in the following paragraphs. The substrates were in thermal contact with liquid-nitrogen-filled copper reservoirs, and they were positioned ~2 mm in front of W-wire filaments, which were used as radiative heating sources. Temperatures were monitored using thermocouple junctions (type K for Pt and W/5%Re−W/26%Re for W) that were spot-welded to the edges of the substrates. Electronic ice points substituted for reference junctions. The uncertainty in temperature measurements was ±0.5 K for the Pt substrate and ±2 K for the W substrate. The substrates were cleaned by argon ion bombardment or oxidation, as appropriate.

Experiments were carried out on ultrathin (0.05−0.10 μm thick), liquid $H_2O + H_2SO_4$ films that were deposited on the substrates. The films were prepared as follows. Pure, crystalline H_2SO_4 films were synthesized by co-condensing H_2O and SO_3 onto the substrates at 100 K and then annealing to 260 K. Such films melt incongruently in vacuo at 285 K to form $H_2O + H_2SO_4$ solutions that contain ~96 wt % H_2SO_4.[36] These extremely concentrated sulfuric acid films can be supercooled in vacuo to 255 K before recrystallizing; in the presence of water vapor the crystallization temperature is even lower. The exposure of a liquid film to water vapor results in H_2O uptake to form an $H_2O + H_2SO_4$ solution of composition dictated by the liquid−vapor coexistence curve. The film compositions cited herein are based upon comparisons of the film infrared spectra with those of reference solutions reported in the literature.[33] Film compositions were also estimated by reference to published vapor pressure curves of the $H_2O + H_2SO_4$ system; below 200 K, the estimates are based on extrapolations of the published curves.[38−40] Composition assignments made using the two methods generally agree to within 2 wt %. Under most of the conditions investigated in this work, the films were supercooled, i.e., they were liquid but metastable with respect to the solid acid.

Because the partial pressures of H_2SO_4 and SO_3 over sulfuric acid are exceedingly low, very little (<5%) of the H_2SO_4 in a sulfuric acid film was lost to evaporation over the course of an experiment (usually 30 or fewer minutes). Since water was constantly replenished to the films from the gas phase, the amount of water in a film, and therefore the film thickness, could be taken as a constant as long as the water pressure and the temperature were unchanging. The film thicknesses (λ_S), which typically were 0.05−0.10 μm, were calculated from the equation:

$$\lambda_S = \lambda^* \cdot \frac{100}{w_S} \cdot \frac{\rho^*}{\rho_S} \qquad (1)$$

In eq 1, λ^* is the thickness of the pure, crystalline H_2SO_4 film used to prepare the sulfuric acid solution, w_S is the film composition expressed as wt % H_2SO_4, and ρ^* and ρ_S are the densities of the pure crystalline acid and the sulfuric acid solution, respectively.[41] Densities are taken from a compilation of data on 293 K sulfuric acid and are not corrected for thermal expansion. The density ratio, ρ^*/ρ_S, ranges between 1.821 for 0 wt % H_2SO_4 and 0.997 for 97 wt % H_2SO_4. In the FTIRAS chamber, λ^* was determined from the intensities of the OH stretching and H_2SO_4 stretching/bending bands, and taking into account the beam path length through a film and the optical constants of sulfuric acid.[42] Values obtained in this way are considered to be crude measures of thickness, with a systematic error of +300%/−75%. In the mass spectrometry chamber, λ^* was determined at the end of an experiment, by measuring the H_2SO_4 yield during the temperature-programmed evaporation/sublimation of a film. The H_2SO_4 yield from a single H_2SO_4 monolayer adsorbed on the substrate surface was also measured. Assuming that the packing efficiency of adsorbed H_2SO_4 is equal to that of bulk sulfuric acid, the thickness (in monolayers) of a film is the ratio of the two evaporation/sublimation yields. A single H_2SO_4 monolayer has a thickness of 4.46×10^{-4} μm; this value is calculated from the density of pure, crystalline H_2SO_4, and it assumes that the solid is isotropic.[43] Thickness measurements obtained in this way are considered to be considerably more reliable than those obtained using FTIRAS, with a systematic error of ±25% and a somewhat smaller random error.

Gases were introduced into the reaction vessels via stainless steel leak valves. For low pressures ($<10^{-5}$ Pa), the entire chamber was backfilled with the gas of interest. For pressures greater than 10^{-5} Pa, gases were introduced via directed dosers. During directed dosing, the sample was positioned directly in front of the tube used to transport gas from behind the leak valve into the reaction vessel. The geometry of the directed doser (and its more sophisticated variant, the double-doser, discussed below) was such that the effective pressure at a sulfuric acid sample was much greater than the pressure rise in the reaction vessel as a whole. This effect could be exploited to achieve effective pressures as high as 10^{-2} Pa at a sulfuric acid sample. The so-called enhancement factor of a doser could be readily determined through suitable calibration experiments, for instance by studying the adsorption of CO on the clean Pt(111) substrate[44] or the condensation of H_2O onto cold (<170 K) water-ice,[45] systems for which the absolute uptake probabilities are well-known. The value of the enhancement factor is a sensitive function of the system geometry, since it rapidly decreases with increasing sample-doser distance. For the experiments described in this work, the enhancement factors of the water dosers were generally ~70. For the acetone dosers, the enhancement factors were somewhat smaller.

Pressures were measured with nude ion gauges, and in the case of water were corrected for the H_2O ionization efficiency. The acetone, mesityl oxide, and trimethylbenzene pressures are uncorrected because their ionization efficiencies are unknown. The pressure uncertainties are largely associated with the uncertain calibration of the ionization gauge, and are estimated as ±25% for water and ±50% for all other species. Deionized water was subjected to multiple osmotic filtrations and, prior to use each day, was degassed using multiple freeze−pump−thaw cycles. Sulfur trioxide (Aldrich, 99%) required special handling procedures that are described elsewhere.[35] Acetone (Fischer, 99.7%), mesityl oxide (Aldrich, 98%), and 1,3,5-trimethylbenzene (Aldrich, 98%) were degassed before use each day and otherwise used as received.

Results

Mass Spectrometric Studies of Acetone Uptake. The kinetics and thermodynamics of acetone uptake were studied using a modification of the King and Wells method.[46] The uptake experiments involved the use of a double-doser designed to provide separately controllable fluxes of acetone and water to the sulfuric acid samples. A schematic diagram of the double-doser is shown in Figure 1. The double-doser consisted of two concentric 0.9 mm-wall stainless steel tubes, the outer diameters of which were 9.5 and 15.6 mm. The inner tube and the annulus between the inner and outer tubes were each connected to UHV leak valves, the other sides of which were attached to the water

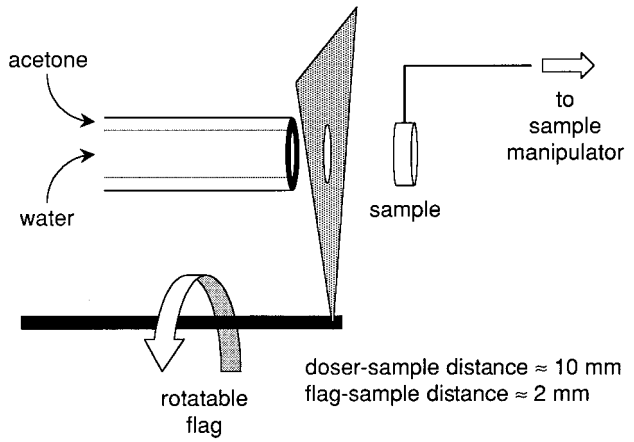

Figure 1. A schematic diagram of the double-doser used for the acetone uptake experiments.

and acetone reservoirs, respectively. During an uptake measurement, the sulfuric acid sample was positioned ~1 cm in front of the double doser. A rotatable flag could be interposed between the sample and the doser. The flag had a circular hole of radius roughly equal to that of the inner tube. The flag could thus be used to prevent most of the incident acetone flux from impinging on the sample, while maintaining a nearly constant water pressure and therefore film composition.

Before presenting the actual uptake data, we consider the two hypothetical uptake curves shown in Figure 2. In the uptake curves, the acetone mass spectral signal (which is proportional to the rate of appearance of gas-phase acetone into the reactor vessel) is plotted versus time. The experiments begin with the acetone source turned off and the flag interposed between the doser and sample. At t_i, the acetone doser is opened. Acetone flows into the reaction vessel, but the flag prevents its interaction with the sulfuric acid sample. Instead, the rapid pumping speed of the UHV chamber ensures that acetone is pumped from the vessel before it impinges upon the sample. At t_{ii}, the flag is rotated away, and acetone begins to impinge upon the sulfuric acid. The pressure drop at t_{ii} is a consequence of the adsorption or absorption of acetone by the sulfuric acid sample. The acetone signal evolves with time until t_{iii}, when the flag is again interposed between the acetone source and the sample. Eventually, the acetone pressure returns to the value it had at t_i. At t_{iv}, the acetone source is turned off, and the acetone signal quickly drops to its background value in the UHV reactor.

It is important to point out that not all of the acetone that enters the reactor between t_{ii} and t_{iii} impinges upon the sulfuric acid sample. Rather, some fraction, F, of the incident acetone is intercepted by the sample; the rest is rapidly pumped from the reaction vessel. For the experiments described in this paper, F was always between 0.2 and 0.6. The exact value of F, which was determined using the same method used to determine the enhancement factor of the water doser, depends on the system geometry. The geometry was not constant throughout the course of the experiments, and so F was reevaluated whenever system geometry was altered. The acetone which never strikes the sulfuric acid sample upon entering the reaction vessel is represented by the shaded regions of the hypothetical uptake curves; in the hypothetical curves, $F = 0.5$.

The uptake curves can be used to determine γ_A, the *net* uptake probability of acetone by sulfuric acid. (The quantity γ_A is a net uptake probability because it is possible for acetone to evaporate or desorb from a sulfuric acid film; γ_A is thus a function of the difference between the acetone absorption/adsorption and evaporation/desorption rates.) In the insets of

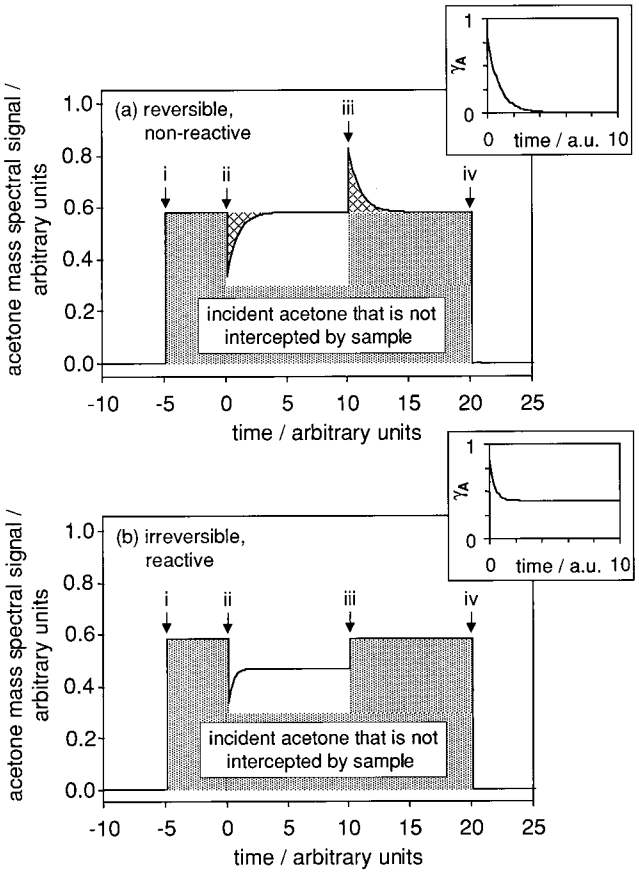

Figure 2. Two hypothetical uptake curves for acetone interacting with sulfuric acid: (a) reversible, nonreactive uptake, and (b) irreversible, reactive uptake. The arrows indicate the times at which (i) the acetone source was turned on with the flag interposed between source and the sample, (ii) the flag was rotated away from the sample, (iii) the flag was rotated back into place, and (iv) the acetone source was turned off. The insets represent a transformation of the hypothetical curves, from a plot of mass spectrometer signal vs time to a plot of net uptake probability (γ_A) vs time, for F (defined in the text) equal to 0.5.

Figure 2, we plot γ_A versus time for the hypothetical uptake curves, starting at $t = 0$, i.e., beginning with acetone exposure to a pure sulfuric acid film. The γ_A values, which in general are a function of time, are obtained from equation 2:

$$\gamma_A(t) = \frac{I_A^0 - I_A(t)}{F \cdot I_A^0} \tag{2}$$

where I_A^0 is the intensity of the acetone mass spectral signal immediately before uptake was allowed to occur, and $I_A(t)$ is the intensity at time t. Equation 2 applies to uptake at any point between t_i and t_{ii}. It assumes, for simplicity's sake, that the background acetone pressure in the reactor is negligible. If the background pressure is not negligible, then I_A^0 in the denominator of eq 1 should be replaced by $(I_A^0 - I_A^b)$, where I_A^b is the background intensity.

In Figure 2, we show two qualitatively different types of uptake curve, one (Figure 2a) for a situation in which uptake is quantitatively reversible and nonreactive, and another (Figure 2b) in which uptake is irreversible and reactive. The former situation would pertain to a system in which acetone was physically dissolved into sulfuric acid. For acetone dissolution, the initial γ_A is equal to the absolute acetone uptake probability in sulfuric acid, because there is no dissolved acetone to evaporate into the gas phase. The value of γ_A rapidly decreases

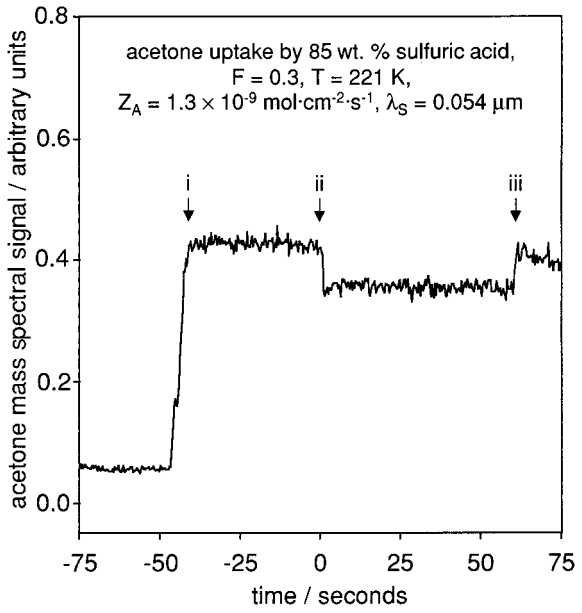

Figure 3. Acetone uptake by 85 wt %, 221 K sulfuric acid. The film thickness was 0.054 μm, Z_A was 1.3×10^{-9} mol cm^{-2} s^{-1}, and F was 0.3. The arrows indicate the times at which: (i) the acetone source was turned on with the flag interposed between source and the sample, (ii) the flag was rotated away from the sample, and (iii) the flag was rotated back into place.

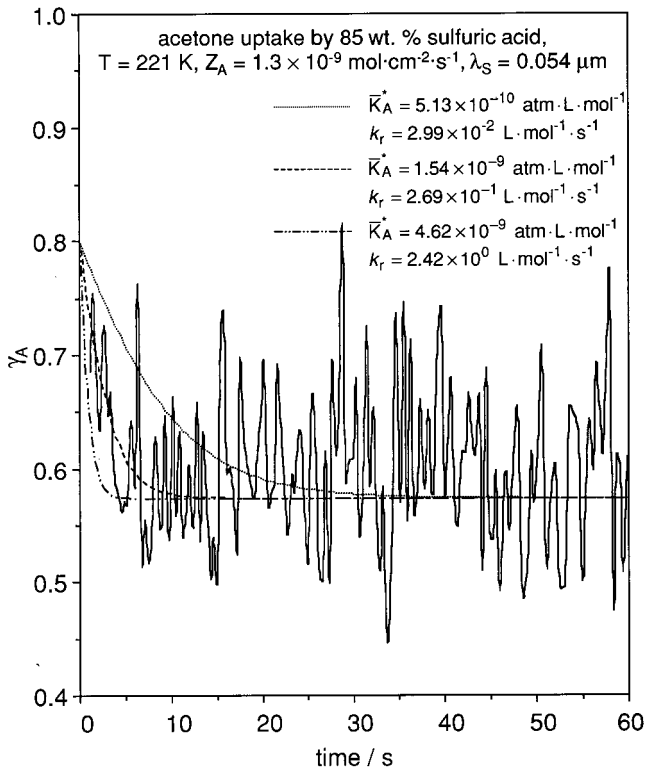

Figure 4. The net acetone uptake probability (γ_A) plotted versus time for 85 wt %, 221 K sulfuric acid. Uptake conditions were $\lambda_S = 0.054$ μm and $Z_A = 1.3 \times 10^{-9}$ mol cm^{-2} s^{-1}. The solid line shows the data; the three broken lines are fits to the data, assuming the $\bar{K}_A^*$ and k_r values indicated in the figure.

with time, however, as acetone accumulates in the film and the evaporation rate becomes ever more rapid. Eventually, the system reaches the acetone solubility limit. At this point, the film is saturated with acetone, the evaporation and dissolution rates are equal, and γ_A is zero. Note what occurs in Figure 2a at t_{iii}: there is a burst in the acetone signal when the flag is again interposed between the sample and the double-doser. This is because the solubility of a gas in a condensed phase is a function of the pressure of that gas. When acetone is no longer allowed to impinge upon the sulfuric acid sample, its solubility drops to zero, and it rapidly evaporates from the film. For situations in which acetone uptake is quantitatively reversible, the areas of the crosshatched regions of the uptake curve must be equal.

The uptake curve in Figure 2b represents what one might expect for a situation in which acetone is irreversibly and reactively absorbed by the sulfuric acid. For such a situation, γ_A never returns to zero because the system does not reach the acetone solubility limit. Rather, acetone is taken up by sulfuric acid only to form a heterogeneous reaction product which, depending on its vapor pressure over sulfuric acid, evaporates or persists in a condensed phase. The time-evolution of γ_A need not be as it is shown in Figure 2: γ_A could, depending on the uptake mechanism, remain constant with time, decrease to zero, or even increase from its initial value. The signature for irreversible uptake is the absence of a burst in the acetone signal at t_{iii}, since it indicates that acetone, once it is taken up by the sulfuric acid, never again evaporates into the gas phase.

As the preceding paragraphs make clear, the uptake curves contain an abundance of information about the nature of the interaction between acetone and sulfuric acid. Other modes of interaction are possible, and each of these modes is associated with a characteristic type of uptake curve. However, we defer a more detailed description of the uptake curves to the Discussion, and proceed instead to the data.

Figure 3 shows an uptake curve that is characteristic of the interaction of acetone with a sulfuric acid film consisting of $\geq$75 wt % H_2SO_4. The conditions during uptake were the following: film temperature = 221 K, w_S = 85 wt %, F = 0.3, and acetone-sample collision rate (Z_A) = 1.3×10^{-9} mol cm^{-2} s^{-1}. (This collision rate corresponds to a pressure of 4.0×10^{-4} Pa.) The film was deposited on the Pt substrate, as were all films studied using the King and Wells method. The experiment began with the acetone doser turned off and the rotatable flag interposed between the sample and doser. As is the case for the hypothetical uptake curves, the arrows at positions i, ii, and iii correspond, respectively, to the times at which acetone is introduced into the reactor, at which the flag is rotated away from the sample, and at which the flag is rotated back into place. The time axis has been defined so that $t_{ii} = 0$ s. The data shown in Figure 3 were used to determine the time-dependent net uptake probability of acetone under this set of conditions; γ_A is plotted versus time in Figure 4. (Also plotted in Figure 4 are the results of three simulations of the γ_A-versus-time curves. The model used to generate the simulated curves is described in the Discussion.) There is considerable scatter in the experimentally determined γ_A values. This is mostly a consequence of the fact that F is a relatively small number, and it points out a limitation of the double-doser design. The fraction of incident acetone which was intercepted by the sample could be made larger by using the central tube of the double-doser as the acetone source. However, it then was impossible to investigate solutions containing <85 wt % H_2SO_4, since relatively little water vapor could be delivered to a sulfuric acid sample through the annulus of the double-doser. We are currently working to improve the design of the double-doser so that more of the incident acetone is intercepted by the sample.

From Figures 3 and 4, it is obvious that acetone uptake by the 85 wt % acid at 221 K is at least partly irreversible. There is an immediate drop in the acetone signal at t_{ii}, when the flag

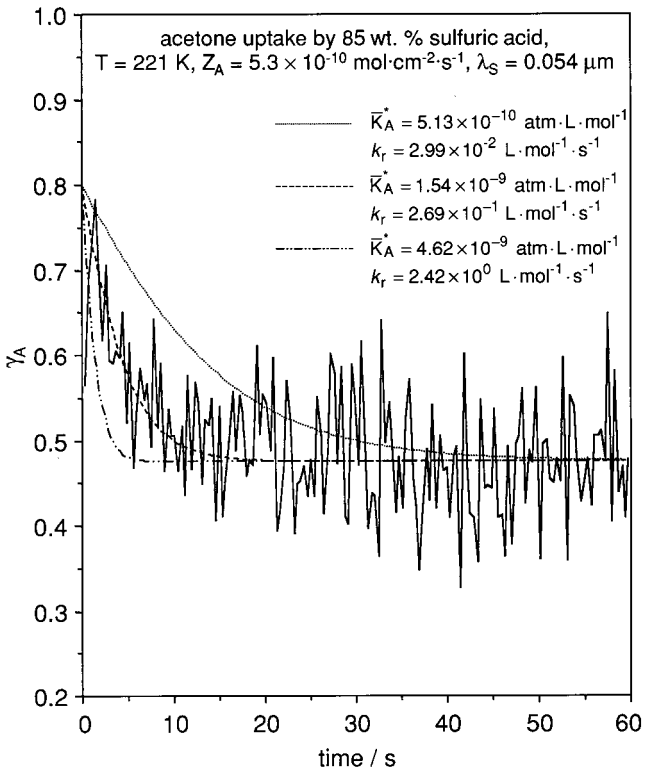

Figure 5. The net acetone uptake probability (γ_A) plotted versus time for 85 wt. %, 221 K sulfuric acid Uptake conditions were: $\lambda_S = 0.054$ μm and $Z_A = 5.3 \times 10^{-10}$ mol cm^{-2} s^{-1}. The solid line shows the data; the three broken lines are fits to the data, assuming the $\bar{K}_A^*$ and k_r values indicated in the figure.

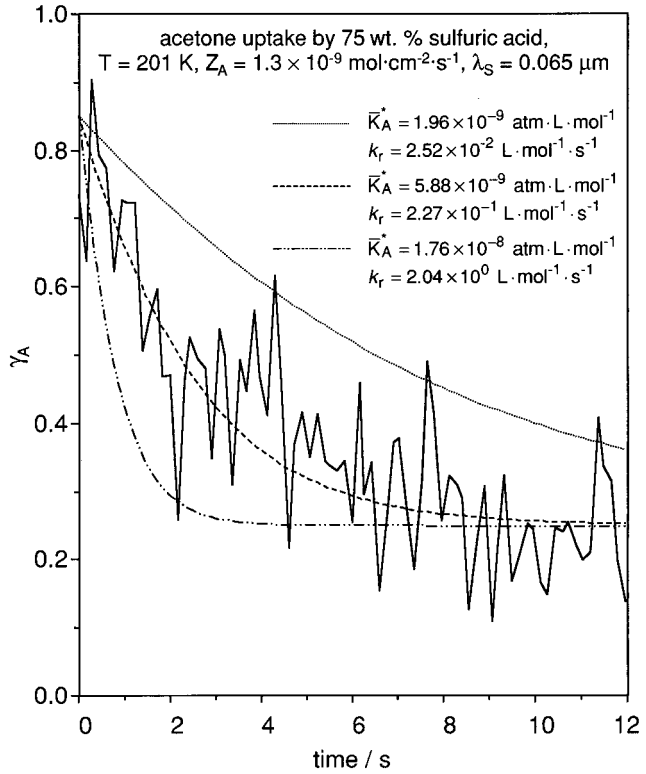

Figure 6. The net acetone uptake probability (γ_A) plotted vs time for 75 wt %, 201 K sulfuric acid. Uptake conditions were $\lambda_S = 0.065$ μm and $Z_A = 1.3 \times 10^{-9}$ mol cm^{-2} s^{-1}. The solid line shows the data; the three broken lines are fits to the data, assuming the $\bar{K}_A^*$ and k_r values indicated in the figure.

is rotated away from the sample. From the signal decrease, we infer that the initial uptake probability (γ_A^0) is 0.8. The signal recovers over a period of roughly 10 s, but not to what it was immediately before acetone was allowed to interact with the sample. Rather, the acetone signal reaches a constant value corresponding to a steady-state loss probability, γ_A^∞, of roughly 0.6. As expected, when the flag is rotated back into place at t_{iii}, the acetone signal increases toward its initial value. Unfortunately, the quality of the data is not adequate to determine whether acetone evaporates from the film after t_{iii}, and, therefore, whether all of the acetone taken up by the sulfuric acid film is irreversibly bound. That is, the slow drop in acetone signal after t_{iii} may be associated with the evaporation of reversibly absorbed acetone from the film, or it could be the result of a decreasing leak rate from the double-doser. We cannot distinguish between these possibilities because it was difficult to maintain an absolutely constant acetone leak rate into the reactor vessel, at least as the double-doser was configured for these experiments. The difficulty of maintaining a constant leak rate was especially acute when large amounts of water were being simultaneously leaked into the reactor, as was the case whenever the $H_2O + H_2SO_4$ mixtures contained <96 wt % H_2SO_4.

Irreversible uptake curves were obtained over broad ranges of film composition (75 −> 96 wt %), temperature (200−225 K), and Z_A ($2 \times 10^{-10} - 2 \times 10^{-9}$ mol cm^{-2} s^{-1}). Details of these experiments are to be reported elsewhere, but in Figures 5 and 6 we plot γ_A versus time for two other sets of conditions. Although all of the irreversible loss data show certain similarities (γ_A^0, for instance, is always ~0.8), a comparison of Figures 4−6 reveals that the kinetics of irreversible acetone loss depend on composition, T, and Z_A. For instance, in an 85 wt %, 221 K film, γ_A^0 is 0.57 for $Z_A = 1.3 \times 10^{-9}$ mol cm^{-2} s^{-1} and 0.48 for $Z_A = 5.3 \times 10^{-10}$ mol cm^{-2} s^{-1}. For a 75 wt % film at 201 K and $Z_A = 1.3 \times 10^{-9}$ mol cm^{-2} s^{-1}, γ_A^0 is 0.25. A 0.05 μm thick, 85 wt %, 221 K film reaches steady-state in roughly 5 s, whereas a 75 wt %, 205 K film of the same thickness requires nearly 10 s to achieve steady state. These observations, which are summarized in Table 1, are all reproducible despite the high degree of scatter in the data, and we conclude that they are statistically significant. An explanation for the composition, temperature, and collision-rate dependence of the irreversible loss probability is given below.

TABLE 1: Summary of the Irreversible Uptake Measurements and the Paramaters Used to Simulate the Uptake Curves[a]

w_S/wt %	T/K	Z_A/mol cm^{-2} s^{-1}	γ_A^0	γ_A^∞	$\bar{K}_A^*$/atm L mol^{-1}	k_r/L mol^{-1} s^{-1}
75	201	1.3×10^{-9}	0.85	0.25	5.9×10^{-9}	2.3×10^{-1}
85	221	5.3×10^{-10}	0.80	0.48	1.5×10^{-9}	2.7×10^{-1}
85	221	1.3×10^{-9}	0.80	0.57	1.5×10^{-9}	2.7×10^{-1}

[a] The symbols w_S, Z_A, γ_A^0, γ_A^∞, $\bar{K}_A^*$, and k_r are defined in the text.

Under certain conditions, acetone uptake is reversible. Figure 7 summarizes the results of an experiment conducted on a 70 wt %, 187 K film for $Z_A = 3.0 \times 10^{-9}$ mol cm^{-2} s^{-1}. For this experiment, F was 0.2. The experiment began with the flag interposed between the sample and the doser. At time $t = 0$ s, the flag was rotated away from the sample, and uptake was allowed to occur. The flag was rotated back into place after ~15 s, rotated away again at ~30 s, and finally rotated back between the sample and doser at ~45 s. In Figure 7, we plot the *apparent* value of γ_A, which was extracted from the uptake curve, versus time. Clearly, uptake by 70 wt %, 187 K sulfuric acid differs in important ways from uptake by the more concentrated, warmer solutions. First, γ_A, which is initially ~0.6,

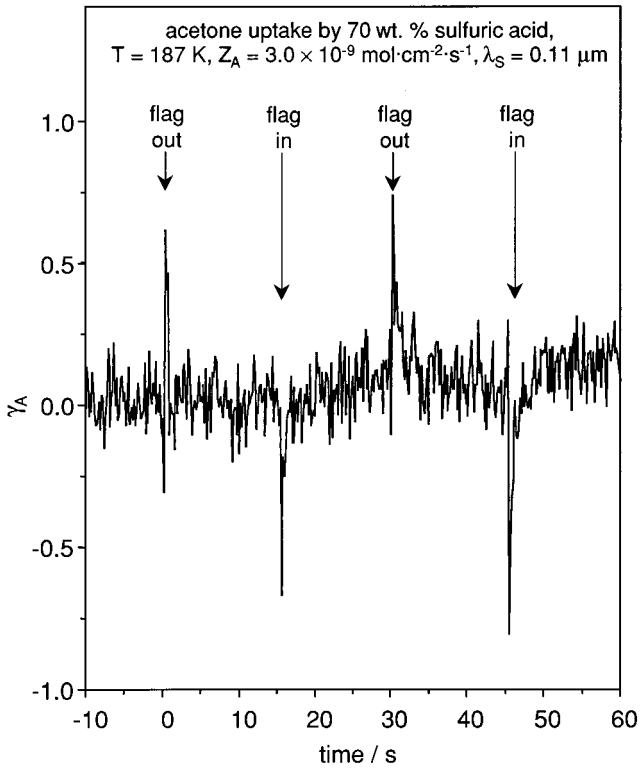

Figure 7. The net acetone uptake probability (γ_A) plotted vs time for 70 wt %, 187 K sulfuric acid. Uptake conditions were $\lambda_S = 0.11$ μm and $Z_A = 3.0 \times 10^{-9}$ mol cm^{-2} s^{-1}. The apparently negative γ_A values are a consequence of the fact that acetone evaporates from a film when the flag is re-interposed between the acetone source and the sulfuric acid sample.

decreases with time to 0 rather than to a nonzero, steady-state value. Second, acetone evaporates from sulfuric acid upon re-interposition of the flag; this is the reason for the apparently negative γ_A values at t =15 and 45 s. Third, the 70 wt % acid evolves much more rapidly toward steady state than do the more concentrated acids: for the 70 wt % acid, γ_A decreases from its initial value to 0 in fewer than 2 s. As we shall see, the origin of this more rapid evolution toward steady state is a reduced acetone solubility.

Since γ_A is proportional to the net rate of acetone uptake, the integral of γ_A with respect to time is proportional to the amount of acetone taken up into a film. The data presented in Figure 7 were numerically integrated using the trapezoid method over the following time intervals: 0−2 s, 15−17 s, 30−32 s, and 45−47 s. The time intervals for the first and third of these integrals correspond to the periods during which acetone was being taken up into the sulfuric acid, and the intervals for second and fourth integrals correspond to the periods during which acetone was evaporating. The values of the first through fourth integrals were 0.287, −0.302, 0.330, and −0.295 s, respectively, for a mean absolute value of 0.304 s with a 6% standard deviation. We conclude that the amount of acetone taken up by sulfuric acid near 0 and 30 s was equal, within experimental error, to the amount that evaporated near 15 and 45 s. Acetone uptake is therefore *quantitatively* reversible under this set of conditions.

Acetone uptake by 70 wt % sulfuric acid was investigated under two other sets of conditions: T = 180 K, $Z_A = 3.0 \times 10^{-9}$ mol cm^{-2} s^{-1}; and T = 195 K, $Z_A = 3.0 \times 10^{-9}$ mol cm^{-2} s^{-1}. For both of these cases, uptake was quantitatively reversible. There were differences in the appearances of the three sets of reversible uptake curves, particularly in the time evolution of γ_A: as T increased, γ_A evolved much more rapidly toward zero. This is a consequence of the fact that the solubilities of gases in liquids decrease with increasing temperature. The integrals of γ_A with respect to time were evaluated for the 180 and 195 K uptake curves just as they were for the 187 K uptake curves. Results are summarized in Table 2, where **I** is the value of the integral. For the high-temperature data, there is considerable uncertainty in the value of **I** because the films were so quickly saturated with acetone.

TABLE 2: Summary of the Reversible Acetone Uptake Measurements and the Calculated Henry's Law Solubility Constants[a]

T/K	γ_A^0	**I**/s	c_A/mol L^{-1}	$\bar{K}_A^*$/atm L mol^{-1} (from eq 3)	$\bar{K}_A^*$/atm L mol^{-1} (from eq 14)
180	0.59	1.9	0.50	1.4×10^{-8}	4.0×10^{-8}
187	0.62	0.30	0.081	8.5×10^{-8}	1.4×10^{-7}
195	0.74	0.064	0.017	4.1×10^{-7}	8.7×10^{-7}

[a] For all of the experiments, the acid composition was 70 wt % H_2SO_4, Z_A was 3.0×10^{-9} mol cm^{-2} s^{-1}, and the film thickness was 0.11 μm. The symbols γ_A^0, **I**, c_A, and $\bar{K}_A^*$, are defined in the text.

FTIR Studies of Acetone and its Reaction Products. The reactions of acetone in sulfuric acid films of varying composition were studied with FTIRAS. In an earlier study,[16] we published infrared difference spectra of sulfuric acid exposed to acetone in the frequency region 1500−1900 cm^{-1}. Protonated acetone (**2**) was identified from the low value of its carbonyl stretching frequency. Protonated mesityl oxide (**3**) and trimethylbenzene (**4**) were identified by comparing the acetone product spectra to those of authentic mesityl oxide and trimethylbenzene samples that had been taken up by sulfuric acid. Literature spectra of mesityl oxide and trimethylbenzene adsorbed on the surfaces of acidic zeolites provided additional support for the product assignments.[47] The FTIRAS results showed that protonated acetone is the sole uptake product in the 70 wt % acid, with the condensation products appearing only for $w_S \geq 75$ wt %.

In the present work, FTIRAS was used to confirm that acetone uptake by the 70 wt % acid is quantitatively reversible, and also to determine the fate of the condensation products **3** and **4**. For these experiments, the sulfuric acid films were exposed to acetone until they reached steady state. At that point, the acetone source was turned off, and infrared spectra were recorded as a function of time. Spectra were recorded in difference mode, with the spectra of the original, pure acid solution serving as the background spectra. These experiments also made use of a double-doser, but of simpler design than that used for the acetone uptake measurements. The double-doser in the FTIRAS chamber consisted of two parallel, tubes, each of which was connected to a leak valve. The tubes were constructed of 12 mm o.d., 0.09 mm wall stainless steel. The centers of the tubes were 2 cm apart.

In Figure 8, we show a series of four infrared difference spectra, which were obtained from a 0.05 μm thick, 96 wt % film deposited on Pt. The sample temperature was 265 K, and Z_A during acetone exposure was 2.4×10^{-10} mol cm^{-2} s^{-1}. Roughly 160 s elapsed between the time at which the film was first exposed to acetone and the time (defined to be $t = 0$) at which acetone exposure was terminated. During this time, less than 5% of the sulfuric acid film evaporated, as determined from the nondifference FTIRAS spectra. In Figure 8, we show spectra recorded at t = 0, 54, 108, 162, and 216 s, where the times correspond to the middle of the data acquisition periods. Approximately 15 s was required to record each spectrum. A single feature is observed in the infrared difference spectra between 1500 and 1700 cm^{-1}. It is a broad band centered at

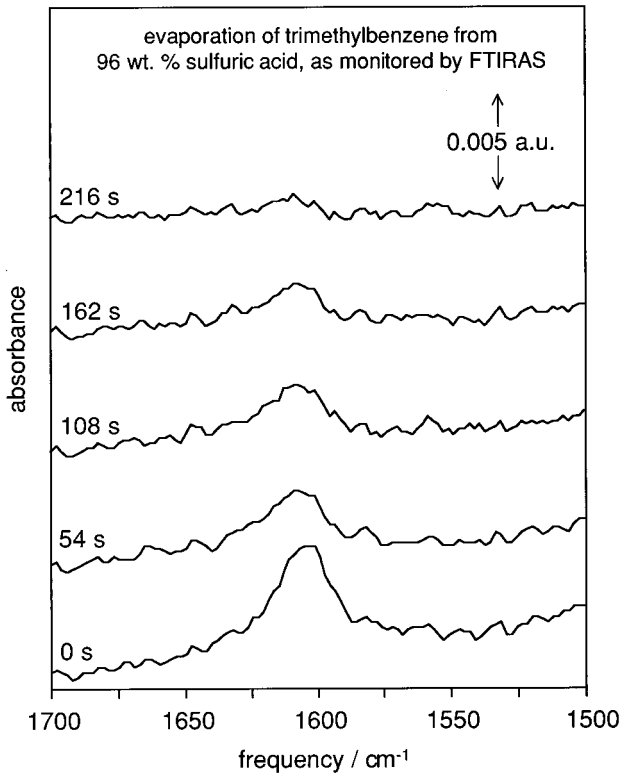

Figure 8. FTIRAS difference spectra recorded during the evaporation of trimethylbenzene from 96 wt % sulfuric acid. The broad feature near 1610 cm^{-1} is associated with a ring-breathing mode of the aromatic C_6 ring of trimethylbenzene. The trimethylbenzene + sulfuric acid mixture was formed by exposing sulfuric acid ($T = 265$ K, $\lambda_s = 0.046$ μm) to acetone ($Z_A = 2.4 \times 10^{-10}$ mol cm^{-2} s^{-1}) for ~160 s.

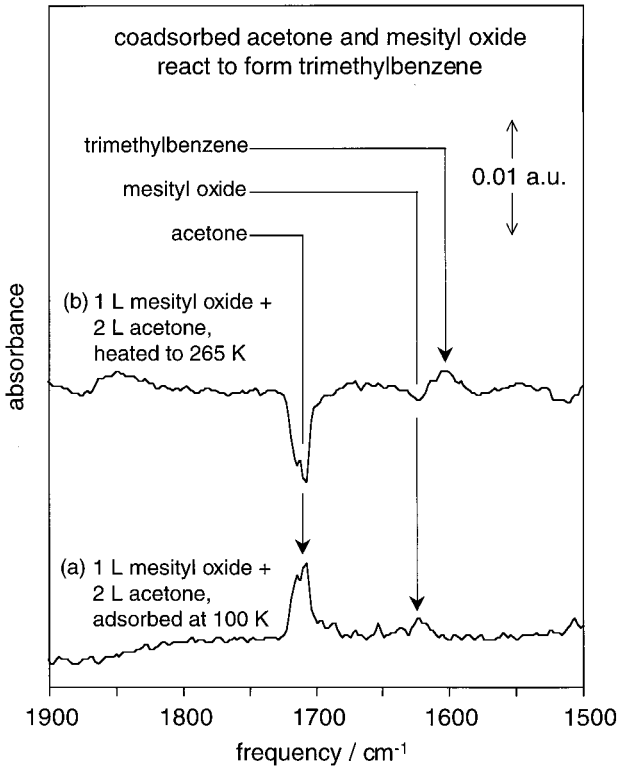

Figure 9. FTIRAS difference spectra of a mesityl oxide + acetone mixture adsorbed on pure, solid H_2SO_4. The mixture was prepared by adsorbing first 1 L of mesityl oxide and then 1 L of acetone. Spectra were recorded (a) immediately after adsorption at 100 K, and (b) after heating the mixture to 265 K and cooling back to 100 K.

1610 cm^{-1}, and it is associated with one of the ring-breathing modes of the aromatic C_6 ring of trimethylbenzene.[48] The band, which is most intense at $t = 0$ s, gradually decreases in intensity with time until 216 s, at which point it is virtually below the detection limit. No new bands appear in this or other regions of the infrared spectra during this period, which implies the evaporation of trimethylbenzene from the films. From the time-dependent FTIRAS data, we infer that the time-scale for complete evaporation under these conditions is roughly 200 s.

Analogous measurements on sulfuric acid films of $w_S < 96$ wt % demonstrate that acetone and its reaction products evaporate much more readily from the more dilute sulfuric acid. For instance, in both the 85 and 70 wt % acids, acetone or its reaction products quantitatively evaporate in less time than it takes to obtain a single infrared spectrum (ca. 15 s). Partly, this may be due to different evaporation kinetics for acetone, mesityl oxide, and trimethylbenzene. However, the trend in evaporation kinetics is also generally consistent with the fact that the viscosity of sulfuric acid increases with w_S.

Infrared spectroscopy was also used to establish that mesityl oxide is an intermediate along the pathway for trimethylbenzene formation from acetone. Figure 9a shows an infrared spectrum of acetone and mesityl oxide coadsorbed on the surface of pure, solid H_2SO_4 at 100 K. The H_2SO_4 film was deposited on Pt. The spectrum was acquired in difference mode, with the spectrum of the pure, solid H_2SO_4 film serving as the background spectrum. The original film thickness was 0.02 μm. Mesityl oxide was adsorbed first, at an exposure of ~1 Langmuir (L), followed by acetone, at an exposure of ~2 L. (A Langmuir corresponds to an exposure of 10^{-6} Torr s and is roughly equivalent to 1 monolayer if the sticking coefficient is unity.) There are two prominent bands in the infrared spectrum, at 1620 and 1715 cm^{-1}. The former band is assigned to the carbonyl stretch in mesityl oxide; it is lower in frequency than that in a simple ketone or aldehyde because the carbonyl group of mesityl oxide is conjugated to a C−C double bond. The higher frequency band is attributed to the carbonyl stretch of acetone. Its frequency is essentially equal to that in condensed acetone because acetone was in this case adsorbed on mesityl oxide, not on sulfuric acid, and there was no opportunity for hydrogen bond formation.

Figure 9b shows an infrared spectrum recorded after slowly heating the mesityl oxide + acetone mixture to 265 K and then cooling back to 100 K. This spectrum was also acquired in difference mode, but with the spectrum of the original mesityl oxide + acetone mixture serving as the background spectrum. Heating to 265 K results in the complete disappearance of the bands associated with acetone and mesityl oxide, and with their replacement by the trimethylbenzene ring-breathing mode at 1610 cm^{-1}. Separate TPD and FTIRAS measurements established that, in the absence of coadsorbed acetone, mesityl oxide does not desorb from or react on pure H_2SO_4 below 265 K. Thus, the disappearance of the mesityl oxide carbonyl stretch between 100 and 265 K is consistent only with a reaction between acetone and mesityl oxide to form the condensation/dehydration product trimethylbenzene.

All of the data presented so far were obtained from films that were deposited on a Pt substrate. To verify that the substrate played no role in the uptake chemistry, we carried out analogous FTIRAS experiments on films that were deposited on the W substrate. In no case did we observe any differences in the reaction product spectra, except for those that could be attributed to the different optical properties of Pt and W. We conclude that the substrate plays no role in the heterogeneous reactions of acetone.

Temperature Programmed Desorption (TPD) Studies of the Acetone Reaction Products. Mesityl oxide and trimethylbenzene were not observed mass spectrometrically during the irreversible acetone uptake measurements. This is presumably a consequence of their slow evaporation from the sulfuric acid films and their extensive fragmentation in the mass spectrometer. Trimethylbenzene evaporation was detected during TPD, however. For the TPD experiments, the sulfuric acid films were first exposed to acetone and then rapidly (ca. 10 s) quenched to 100 K. They then were heated at rates of $2-10$ K s^{-1}, and the gas-phase products were detected mass spectrometrically. Figure 10 summarizes the results of one such an experiment. In this case, the sulfuric acid film, which was deposited on a Pt substrate, contained 96 wt % H_2SO_4. Z_A during acetone exposure was 5.1×10^{-12} mol cm^{-2} s^{-1}, and the exposure time was 120 s. Trimethylbenzene, which was detected as its molecular ion (*m*/*e* 120) and as a number of abundant ion fragments, was the sole observed reaction product. It evolves into the gas phase during TPD near 320 K, and its evolution is coincident with H_2SO_4 sublimation/evaporation. Figure 10 shows only the leading edge of H_2SO_4 sublimation/evaporation peak because the H_2SO_4 yield was sufficient to saturate the *m*/*e* 80 channel of the mass spectrometer detector.

Neither acetone (detected as *m*/*e* 43) nor mesityl oxide (*m*/*e* 55) was observed during TPD. Their absence can be understood as a consequence of the fact that heating an $H_2O + H_2SO_4$ mixture in vacuo results in the preferential evaporation of H_2O, and therefore in the formation of a progressively more concentrated acid. This effect is manifested in TPD spectra of $H_2O + H_2SO_4$ mixtures, which show a broad H_2O evolution feature leading up to the H_2SO_4 sublimation/evaporation peak. A sulfuric acid film therefore consists of nearly pure H_2SO_4 at the onset of product release during TPD. The pure acid is a medium that, according to FTIRAS, is active for the quantitative conversion of absorbed acetone to trimethylbenzene.

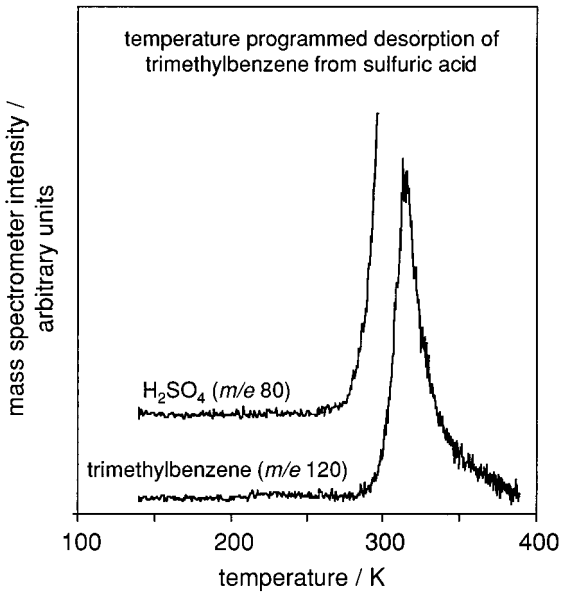

Figure 10. Temperature-programmed desorption (TPD) of trimethylbenzene from a sulfuric acid film. Products detected were trimethylbenzene (*m*/*e* 120) and H_2SO_4 (*m*/*e* 98). The film was prepared by exposing sulfuric acid ($w_S = 96$ wt %, $T = 100$ K, $\lambda_s = 0.046$ μm) to acetone ($Z_A = 2.4 \times 10^{-10}$ mol cm^{-2} s^{-1}) for ~120 s, and then rapidly quenching to 100 K. The heating rate during TPD was ~5 K s^{-1}.

Discussion

Overview. The results we present here are consistent with those described in an earlier, much briefer study of the acetone + sulfuric acid system.[37] In our earlier work, which mostly concerned FTIRAS studies of ultrathin sulfuric acid films exposed to acetone, we suggested a pathway for trimethylbenzene formation from acetone (see Scheme 1), and we demonstrated that the extent to which acetone reacts is a function of the sulfuric acid composition and temperature. The new uptake measurements agree with these earlier findings in that they imply purely reversible uptake in 70 wt % sulfuric acid and substantial reactive uptake in the more concentrated sulfuric acid films. The new infrared studies, especially those concerning acetone and mesityl oxide coadsorbed on solid sulfuric acid, demonstrate that mesityl oxide is an intermediate for trimethylbenzene from acetone. Although adsorbed layers on a solid surface obviously differ in important ways from dissolved molecules in a liquid solution, it would be very surprising for different trimethylbenzene formation mechanisms to be operative in these two media. Finally, the TPD results shown in Figure 10 provide mass spectrometric confirmation of trimethylbenzene formation from acetone.

The new data in this work also allow us to extend and to refine our understanding of the heterogeneous interactions between acetone and sulfuric acid. As we describe below, we are able to determine Henry's law solubility constants for acetone in 70 wt % sulfuric acid, and also, from the temperature dependence of the solubility constants, to estimate values for the enthalpy and entropy of acetone solution. Furthermore, using a simple, two-step kinetic model to describe the acetone condensation reactions, we are able to determine Henry's law solubility constants and condensation rate constants of acetone in 75−85 wt % sulfuric acid. Taken together, the results and their analysis shed considerable light on the origin of sulfuric acid's decreased reactivity below 75 wt %. In particular, they suggest that mesityl oxide and trimethylbenzene formation do not occur in the 70 wt % acid, not because of an intrinsic decrease in the acid reactivity, but because of a steep drop in acetone's solubility. The results thus may have potentially important implications for the interactions of other organic compounds with tropospheric sulfuric acid particles, since such particles tend to have compositions of 70 wt % and lower.

Uptake Thermodynamics. The reversible uptake curves can be used to determine the solubility of acetone in sulfuric acid. If c_A is the solubility of acetone in sulfuric acid, then for reversible uptake

$$c_A = \frac{Z_A A_S \int_0^\infty \gamma_A(t)\mathrm{d}t}{A_S \lambda_S} \qquad (3)$$

where Z_A is the collision rate of acetone with the $H_2O + H_2SO_4$ sample, A_S is the cross-sectional area of the sulfuric acid sample, and $\int_0^\infty \gamma_A(t)\ \mathrm{d}t$ is the time-integrated uptake probability beginning with a pure $H_2O + H_2SO_4$ film. For purely reversible uptake, a sulfuric acid film will eventually become saturated with acetone, and so the numerator of the fraction on the right side of eq 3 represents the total amount of acetone taken up by sulfuric acid at saturation. The collision rate is equal to the acetone pressure, P_A, multiplied by a constant that is a function of the acetone molar mass (M_A) and the system temperature (T). Moreover, the integral in eq 3 may be replaced by the experimentally determined quantity, **I**, leading to the expression

$$c_A = \frac{P_A \mathbf{I}}{\lambda_S}\left(\frac{1}{2\pi M_A RT}\right)^{1/2} \quad (4)$$

Equation 4 was used to determine the solubility of acetone in 70 wt % sulfuric acid at 180, 187, and 195 K, at an acetone pressure of 7.9×10^{-4} Pa. Results are summarized in Table 2. Under the conditions explored in this work, c_A is in the range $0.02-0.5$ mol L^{-1}.

Solutions of gas i in liquid y may be described by the equation[49]

$$f_i = K_{i,y} \cdot \Gamma_{i,y} \cdot \chi_{i,y} \quad (5)$$

where f_i is the fugacity of the gas, and $K_{i,y}$, $\Gamma_{i,y}$, and $\chi_{i,y}$ are, respectively, the Henry's law constant, activity coefficient, and mole fraction of i in a solution of i and y. In the limit of infinitely low dilution, the activity coefficient becomes unity, and eq 5 reduces to a statement of Henry's law as it is rigorously defined by classical thermodynamics to account for purely physical solubility. For systems in which dissolution involves a chemical transformation of the solute (as is the case for acetone in sulfuric acid, since acetone is protonated), $K_{i,y}$ in eq 5 is replaced by $K^*_{i,y}$, where $K^*_{i,y}$ is the *effective* Henry's law constant. To obtain Henry's law coefficients for the acetone + sulfuric acid solutions considered in this work, we make three assumptions: first, that the acetone pressure is so low that its fugacity can be approximated by its pressure; second, that the acetone concentration is low enough that its activity coefficient may be set equal to unity; and third, that the acetone concentration is low enough that its mole fraction is proportional to its molarity. The second assumption is dangerous given the relatively high equilibrium acetone concentrations cited above. However, the solubility trends reflected in the temperature- and composition-dependent Henry's law constants will no doubt still be valid. The assumption that the acetone mole fraction is proportional to its molarity in the solution allows the acetone concentration to be expressed more conveniently, in units of molarity rather than as a mole fraction. After making these approximations and rearranging eq 5, we obtain

$$P_A \approx K_A^* c_A \left\{\frac{M_{H_2SO_4} M_{H_2O}}{\rho_S[M_{H_2SO_4} - (w_S/100)(M_{H_2SO_4} - M_{H_2O})]}\right\} \quad (6)$$

where P_A is the acetone vapor pressure over an acetone + sulfuric acid solution of acetone molarity c_A and effective Henry's law constant K_A. In eq 6, $M_{H_2SO_4}$ and M_{H_2O} are the molar masses of H_2SO_4 and H_2O. The first and third terms of the product on the right side of eq 6 can be combined to yield the much simpler expression:

$$P_A \approx \bar{K}_A^* c_A \quad (7)$$

where $\bar{K}_A^*$ is the effective Henry's law constant of acetone and sulfuric acid for concentrations expressed as the acetone molarity.

From eq 7 and the solubility measurements, $\bar{K}_A^*$ was determined for 70 wt % sulfuric acid at 180, 187, and 195 K. Results are summarized in Table 2. Film thickness is the biggest source of uncertainty in the Henry's law constant measurements, since the terms in P_A cancel when eq 7 is divided by eq 4. We therefore estimate that the percent uncertainty in $\bar{K}_A^*$ is equal to that in λ_S, i.e., ±25%. A plot of $\ln(\bar{K}_A^*)$ versus reciprocal temperature is linear, as expected (Figure 11). From the slope of the van't Hoff plot, we infer that the standard state enthalpy

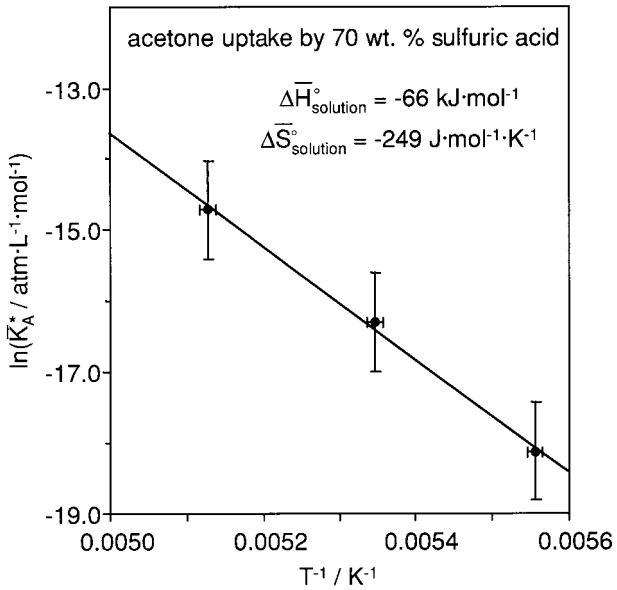

Figure 11. A van't Hoff plot showing the variation of $\ln(\bar{K}^*)$ with T^{-1} for 70 wt % sulfuric acid. The error bars reflect that the uncertainties in $\bar{K}_A^*$ and T are ±25% and ±1 K, respectively. $\Delta\bar{H}^\circ_{solution}$ and $\Delta\bar{S}^\circ_{solution}$ were determined from a linear regression analysis of the data, as described in the text.

change of acetone solution in 70 wt % sulfuric acid is -66 ± 10 kJ mol^{-1}. This value may be compared to $\Delta\bar{H}^\circ_{solution}$ for acetone in liquid water at 298 K, which is -53 kJ mol^{-1}.[1] To the extent that the difference between these two quantities is statistically significant, it probably reflects that acetone dissolves in sulfuric acid to form a protonated species, whereas acetone dissolution in liquid water results in the formation of a more weakly absorbed hydrogen-bonded complex. The solution enthalpy of acetone in sulfuric acid certainly exceeds what one would expect for a hydrogen-bonded solute, even allowing for dispersive interactions between the solute and solvent. The standard state entropy change of acetone solution may also be obtained from a van't Hoff plot. The simplest way to do this is by plotting the logarithm of K_A^* (rather than of $\bar{K}_A^*$) versus reciprocal temperature. The y-intercept of such a plot is equal to $\Delta\bar{S}^\circ/R$, where $\Delta\bar{S}^\circ$ is the molar entropy of solution and R is the gas constant. (The data are replotted so that ΔS° is associated with the appropriate gas-phase and solution standard states, which are, respectively, the pure gas at 1 bar pressure, and a hypothetical solution containing pure acetone but with the properties of acetone in an infinitely dilute solution.) We find that $\Delta\bar{S}^\circ$ is -250 ± 50 J mol^{-1} K^{-1}. The negative value reflects that acetone is transferred from the gas phase to a condensed phase. The value is somewhat more negative than that associated with acetone dissolution in liquid water at 298 K, for which $\Delta\bar{S}^\circ$ was reported to be -150 J mol^{-1} K^{-1}.[1] This, too, is probably a consequence of the fact that acetone is protonated in sulfuric acid, since the solvation sphere around an ionic species is likely to be more ordered than that around a neutral one.

Uptake Kinetics. The uptake curves also provide information about the kinetics of acetone uptake. The reversible and irreversible loss curves can be analyzed in terms of similar mechanisms. For reversible loss, we assume that the uptake mechanism is adequately described by a single, reversible step:

$$\text{step 1: } A_{(g)} + H_2SO_{4(l)} \rightleftarrows AH^+_{(l)} + HSO^-_{4(l)} \quad (8)$$

where $A_{(g)}$ represents gas-phase acetone and $AH^+_{(l)}$ is protonated

acetone in solution. We write step 1 with H_2SO_4 as the H^+ source because H_2SO_4 is more abundant and more acidic than H_3O^+ and HSO_4^-, the two other possible proton sources in this system. In any case, the substitution of protonated water or bisulfate has no effect on the overall expression we derive to explain the observed uptake kinetics (vide infra), since during any one experiment the acid composition (i.e., the H_2SO_4/HSO_4^-/SO_4^{2-}/H_2O/H_3O^+ ratio) is unchanging. For irreversible uptake, we add a second, irreversible step:

$$\text{step 2: } AH^+_{(l)} + AH^+_{(l)} \rightarrow C \tag{9}$$

where C indicates the initial condensation product, which we assume is formed via a bimolecular step. We neglect gas- and liquid-phase diffusion in this kinetic analysis. The former phenomenon may be neglected because the system pressures were always so low that gas-phase transport was in or very near the molecular flow regime. Liquid-phase diffusion may be reasonably neglected because the films are so thin; as a result, the concentration of dissolved acetone is everywhere constant. Under the conditions investigated in this work, the time required to saturate a film with acetone was 2 s at most. For acetone to thermally diffuse a distance of 0.05 μm in 10 s, the Fick's law diffusion constant, D_A, must be $\sim 3 \times 10^{-13}$ cm^2 s^{-1}, which is well within the range of values considered reasonable for such systems. For instance, using the parametrization suggested by Williams and co-workers,[50,18] we estimate that D_A is 3.8×10^{-10} cm^2 s^{-1} in the 70 wt %, 200 K acid. The assumption of rapid diffusion is also consistent with the time-dependent FTIRAS measurements of $\leq$85 wt % sulfuric acid, which showed that acetone and its reaction products remain absorbed in an ultrathin film for an average of 2 s or fewer before evaporating into the gas phase. (In the more concentrated and viscous >85 wt % acid, the rapid diffusion assumption does not apply since FTIRAS measurements imply that trimethylbenzene persists for several minutes on average before evaporating.)

We now present a kinetic analysis of irreversible acetone uptake, assuming the above two-step mechanism. The rate expression for reversible uptake, which is a special case of the two-step mechanism, can be determined by setting the rate of step 2 equal to zero. We write the rate of the forward reaction in step 1 (in units of mol cm^{-3} s^{-1}) as $Z_A S_A/\lambda_S$, where Z_A is the gas−surface collision rate in units of mol cm^{-2} s^{-1}, S_A is the absolute adsorption/absorption probability, and λ_S is the film thickness in cm. Although S_A must in general be a function of concentration, we take it as a concentration-independent quantity, since even in a saturated solution the mole fraction of acetone is very small. To obtain a rate expression for the reverse of step 1, we assume that the acetone + sulfuric acid solutions exhibit ideally dilute behavior, from which it follows that the acetone evaporation rate is proportional to concentration. Under such conditions, the rate of acetone evaporation is $\{Z_A S_A/\lambda_S\}$-$\{[AHO(^+_{(l)})]/[AHO(^+_{(l)})]_{eq}\}$, where $[AHO(^+_{(l)})]_{eq}$ is the equilibrium concentration at the temperature and acetone pressure of interest. The evaporation rate term may be further simplified, since $[AHO(^+_{(l)})]_{eq}$ is, according to Henry's law, proportional to the acetone partial pressure at equilibrium. We set the rate of step 2 equal to $k_r[AH^+_l]^2$, where k_r is the second-order rate constant for condensation. After taking into account the source term and the two sink terms for AH^+_l, we obtain the following differential rate expression:

$$d[AH^+_{(l)}]/dt = \left(\frac{Z_A S_A}{\lambda_S}\right)\left(1 - \frac{\bar{K}^*_A[AH^+_{(l)}]}{P_A}\right) - k_r[AH^+_{(l)}]^2 \tag{10}$$

Equation 10 may be integrated analytically to solve for $[AH^+_{(l)}]$. If the initial concentration is zero, then at time t:

$$[AH^+_{(l)}] = \frac{(P_A/\bar{K}^*_A)\{1 - e^{-[(S_A Z_A \bar{K}^*_A qt)/(\lambda_S P_A)]}\}}{\left(\frac{1+q}{2}\right) - \left(\frac{1-q}{2}\right)e^{-[(S_A Z_A \bar{K}^*_A qt)/(\lambda_S P_A)]}} \tag{11}$$

where:

$$q = \sqrt{1 + \left(\frac{4k_r(P_A/\bar{K}^*_A)^2\lambda_S}{S_A Z_A}\right)} \tag{12}$$

We now derive an expression for γ_A, the net acetone uptake probability, as a function of time. The net uptake rate is the difference between the acetone accommodation rate ($S_A Z_A/\lambda_S$) and the evaporation rate $\{(Z_A S_A/\lambda_S)[AH^+_{(l)}]/[AH^+_{(l)}]_{eq}\}$, whereas the maximum uptake rate is simply Z_A/λ_A. Since γ_A is the ratio of these two rates:

$$\gamma_A = S_A\left\{\frac{(q-1) + (q+1)e^{-[(S_A Z_A \bar{K}^*_A qt)/(\lambda_S P_A)]}}{(q+1) + (q-1)e^{-[(S_A Z_A \bar{K}^*_A qt)/(\lambda_S P_A)]}}\right\} \tag{13}$$

Equation 13 provides the basis for the balance of this kinetic discussion, since it provides a formulation for understanding the origin of the time-dependent uptake measurements such as those shown in Figures 4−7.

Consider now the limiting case of reversible acetone uptake. For reversible uptake, $k_r = 0$, $q = 1$, and eq 13 reduces to

$$\gamma_A = S_A e^{-[(S_A Z_A \bar{K}^*_A t)/(\lambda_S P_A)]} \tag{14}$$

A plot of $\ln(\gamma_A)$ versus reciprocal temperature should be linear, with a y-intercept equal to $\ln(S_A)$ and a slope equal to $-(S_A Z_A \bar{K}^*_A)/(\gamma_S P_A)$. The film thickness is a known quantity, and the ratio Z_A/P_A is very nearly a constant (its temperature dependence may be neglected over the temperature range considered in this work), since the collision rate and pressure of a gas are related to each other. Equation 14 suggests a useful and efficient way of determining $\bar{K}^*_A$. Such a method is in fact less practical than that based on the integrated uptake curves, because the 70 wt % films saturate so rapidly with acetone that we are able to obtain very few data points between t_i and saturation. There are only two ways of increasing the number of data points: by increasing λ_S, or by increasing the data acquisition rate. Since the former would have increased the gas load on the vacuum chamber and the latter would have decreased the signal-to-noise ratio of the mass spectrometer signal, neither was an acceptable alternative. Nevertheless, as a check, we did plot $\ln(\gamma_A)$ versus time for the reversible uptake curves. The plots were linear, as expected, and the slopes yielded values for the Henry's law solubility constants that were in reasonable agreement with those obtained from the integrated uptake curves (Table 2). Agreement was best for the lower temperature films, which took longer to become saturated with acetone. In any case, the reasonable agreement between the differently obtained $\bar{K}^*_A$ values suggests the simple uptake model presented above adequately describes the acetone uptake kinetics.

Analysis of the irreversible uptake curves was somewhat more complex, and it involved fitting the experimentally determined uptake curves to eq 13. The two-step acetone uptake model invokes three elementary rate constants, all of which appear in eq 13: S_A, $\bar{K}^*_A$, and k_r. (Strictly speaking, $\bar{K}^*_A$ is not a rate constant, but we treat it as one here because it is used to calculate

the acetone evaporation rate from an acetone + sulfuric acid solution.) Equation 13 also contains the parameter q, as well as the experimentally measured quantities P_A and λ_S. Both S_A and q can be extracted from the initial and steady-state regions of the uptake curves. S_A is equal to γ_A^0, and from eq 13 it follows that at steady-state (i.e., at $t = \infty$):

$$q = \frac{1 + (\gamma^\infty/S_A)}{1 - (\gamma^\infty/S_A)} \tag{15}$$

For the irreversible uptake measurements reported in this work, S_A was always ~0.8, and $1.5 < q < 6.5$. Taking the above discussion into account, we see that $\bar{K}_A^*$ and k_r are the only unknown quantities in eq 13. Moreover, eq 12 defines a strict functional relationship between $\bar{K}_A^*$ and k_r. We thus fit the experimentally determined uptake curves to a *single* adjustable parameter, which we chose to be $\bar{K}_A^*$.

Results of the fitting procedure are illustrated in Figures 4−6, which compare the simulated and the experimentally measured uptake curves. In each of the figures, we show three simulated curves: a best fit and two others, in which the $\bar{K}_A^*$ was either tripled or reduced by a factor of 3 from that in the best fit. The fits are very robust, since modest changes in $\bar{K}_A^*$ from the best-fit value significantly degrade the goodness of fit. Also, the fits are of high quality: the extrema are well predicted, as is the time evolution of γ_A between initial uptake and steady state. Note as well that the two-step uptake model successfully predicts that γ^∞ depends on the acetone partial pressure, at least for the 85 wt %, 221 K acid. The model predicts such a dependence because the acetone reaction (eq 9) is predicted to be second-order in AH^+ concentration, whereas acetone evaporation (eq 8 in reverse) is first-order in $[AH^+]$. Increasing the acetone pressure therefore results in a higher condensation/dehydration probability, and a larger γ^∞ value. An uptake model which invoked a simple first-order acetone loss step would predict that γ^∞ is independent of pressure.

Table 1 summarizes the values we measured for S_A, $\bar{K}_A^*$, and k_r for the conditions explored in this work. As expected, S_A is virtually independent of acid composition and temperature, and it is always very close to unity. The Henry's law solubility constants are 5.9×10^{-9} atm L mol^{-1} for the 75 wt %, 201 K acid and 1.5×10^{-9} atm L mol^{-1} for the 85 wt %, 221 K acid. For the 70 wt % acid, $\bar{K}_A^*$ would almost certainly be much larger at these temperatures: extrapolation of the van't Hoff plot in Figure 11 implies that the 201 and 221 K solubility constants in 70 wt % sulfuric acid are 6.7×10^{-7} and 2.4×10^{-5} atm L mol^{-1}, respectively. The trend we observe, of decreasing $\bar{K}_A^*$ with increasing w_S, has been reported by others.[51] Presumably, the trend's origin is in the increased acidities of the higher w_S solutions, since more acidic solutions would drive the pseudo-equilibrium represented by eq 7 farther to the right. This would result in larger acetone solubilities and, therefore, in smaller $\bar{K}_A^*$ values.

The rate constants for acetone condensation (eq 9) are 0.23 L mol^{-1} s^{-1} in the 75 wt %, 201 K acid and 0.27 L mol^{-1} s^{-1} in the 85 wt %, 221 K acid. Are the rate constants physically reasonable? The diffusion-controlled rate constant for a bimolecular self-reaction of singly charged electrolytes may be estimated using the expression derived by Debye.[52] (The diffusion-limited rate constants establish upper bounds on k_r.) We treat protonated acetone as a sphere of radius 7 Å, and we assume that the parametrization developed by Williams and coworkers[18] adequately describes the viscosity of sulfuric acid at the temperatures and compositions of sulfuric acid investigated in this work. (The latter assumption is a dangerous one, because the parametrization was developed to describe acids of $w_S < 70$ wt %. Nevertheless, it provides the best existing means of estimating sulfuric acid viscosity at these temperatures.) Using the Debye expression, we estimate that the diffusion-limited rate constants for acetone self-condensation in the 75 wt %, 201 K and 85 wt %, 221 K acids are 460 and 530 L mol^{-1} s^{-1}, respectively. Thus, to the extent that the k_r values we measure are ~3 orders of magnitude below the diffusion-limited rate constants, they are reasonable. It is surprising that k_r changes so little between 201 and 221 K. This implies one of three things: (1) a low activation energy for the reaction, (2) a rate constant that increases with decreasing w_S, or (3) a reaction that is nearly diffusion controlled. Further experimental work to clarify this issue is underway.

Atmospheric Implications. This work establishes that sulfuric acid is a reactive medium for acetone. The ability of sulfuric acid to catalyze and promote condensation and dehydration reactions of organic compounds has long been appreciated. However, most of our understanding of such reactions is derived from studies of the ~96 wt % acid at or near room temperature.[53] These studies have focused almost exclusively on the solution-phase chemistry of sulfuric acid, and very little work has addressed the kinetic and thermodynamic barriers that may exist for transport of organic reactants from the gas phase to the surface and from the surface to the solution. Because gas-to-surface and surface-to-solution transport are necessary steps for any heterogeneous atmospheric reaction, a better understanding of these phenomena is highly desirable. Here we present evidence for a sulfuric acid-catalyzed reaction that involves accommodation from the gas phase, and which occurs in relatively dilute (i.e., <96 wt %), low-temperature solutions.

Acetone is an important constituent of the troposphere, and so an obvious question is whether sulfuric acid aerosol particles are a significant source of heterogeneous reactivity for acetone. The studies described in this paper are of greatest relevance to the chemistry of the remote, upper troposphere, where acetone is abundant (~3000 parts per trillion volume, or ~10^{-4} Pa)[54] and there are large numbers of sulfuric acid particles containing <70 wt % H_2SO_4.[40] Because we observe no mesityl oxide or trimethylbenzene formation in solutions of $w_S < 75$ wt %, we conclude that $H_2O + H_2SO_4$ particles are *not* an important reactive sink for acetone in the remote, upper troposphere. Moreover, the Henry's law solubility constants imply that very little dissolution would occur above 200 K, and we infer that physical uptake is unimportant as well.

Acetone is not the sole organic constituent of the troposphere, and so a larger question is whether tropospheric sulfuric acid particles catalyze or promote reactions of other organic compounds. Our kinetic modeling results suggest that there are three important contributors to net reactivity in these types of system: the Henry's law solubility of the reactant, the partial pressure of the reactant, and the rate constant for the reaction itself. (The second of these factors, i.e., the reactant pressure, is important only for heterogeneous processes involving a second- or higher-order loss step, such as that shown in eq 9.) A critical question raised by the present study, then, is this: Why does acetone fail to react in the 70 wt % acid? The results we report here clearly suggest that $\bar{K}_A^*$ is a much more sensitive function of composition than is k_r. Thus it may be that the 70 wt % acid is unable to support significant heterogeneous acetone loss because the solubility of acetone is so low, not because there is a change in the intrinsic reactivity

of the acid between 75 and 70 wt %. One might speculate that organic compounds that are more soluble than acetone or are present at higher concentrations may undergo heterogeneous loss in acids of $w_S < 70$ wt %. That possibility is currently the subject of investigation in our laboratory.

Acknowledgment. This work was supported by the National Science Foundation through Grant CHE-9527665 and the Petroleum Research Fund through Grant PRF-30653-AC5.

References and Notes

(1) Nathanson, G. M.; Davidovits, P.; Worsnop, D. R.; Kolb, C. E. *J. Phys. Chem.* **1996**, *100*, 13007−13020.
(2) Knox, C. J. H.; Phillips, L. F. *J. Phys. Chem. B* **1998**, *102*, 8469−8472.
(3) Taylor, R. S.; Garrett, B. C. *J. Phys. Chem. B* **1999**, *103*, 844−851.
(4) Wayne, R. P. *Chemistry of Atmospheres*, 2nd ed.; Oxford University Press: New York, 1991.
(5) Davidovits, P.; Jayne, J. T.; Duan, S. X.; Worsnop, D. R.; Zahniser, M. S.; Kolb, C. E. *J. Phys. Chem.* **1991**, *95*, 6337−6340.
(6) Saecker, M. E.; Nathanson, G. M. *J. Chem. Phys.* **1994**, *100*, 3999−4005.
(7) Benjamin, I.; Wilson, M. A.; Pohorille, A.; Nathanson, G. M. *Chem. Phys. Lett.* **1995**, *243*, 222−228.
(8) Ronk, W. R.; Kowalski, D. V.; Manning, M.; Nathanson, G. M. *J. Chem, Phys.* **1996**, *105*, 4397−4397.
(9) King, M. E.; Fierhrer, K. M.; Nathanson, G. M.; Minton, T. K. *J. Phys. Chem. A* **1997**, *101*, 6556.
(10) Tribe, L.; Manning, M.; Morgan, J. A.; Stephens, M. D.; Ronk, W. R.; Treptow, E.; Nathanson, G. M.; Skinner, J. L. *J. Phys. Chem. B* **1998**, *102*, 206−211.
(11) Eisenthal, K. B. *Acc. Chem. Res.* **1993**, *26*, 636−643.
(12) Eisenthal, K. B. *Chem. Rev.* **1996**, *96*, 1343−1360.
(13) Baldelli, S.; Schnitzer, C.; Schultz, M. J. *Chem. Phys. Lett.* **1999**, *302*, 157−163.
(14) Baldelli, S.; Schnitzer, C.; Schultz, M. J.; Campbell, D. J. *J. Phys. Chem. B* **1997**, *101*, 10435−10441.
(15) Baldelli, S.; Schnitzer, C.; Schultz, M. J. *J. Chem. Phys.* **1998**, *108*, 9817−9820.
(16) Govoni, S. T.; Nathanson, G. M. *J. Am. Chem. Soc.* **1994**, *116*, 779−780.
(17) Klassen, J. K.; Nathanson, G. M. *Science* **1996**, *273*, 333−335.
(18) Klassen, J. K.; Hu, Z. J.; Williams, L. R. *J. Geophys. Res.* **1998**, *103*, 16197−16202.
(19) Nathanson, G. M. Personal communication.
(20) Hanson, D. R.; Mauersberger, K. *J. Phys. Chem.* **1990**, *94*, 4700−4705.
(21) Abbatt, J. P. D. *J. Geophys. Res.* **1995**, *100*, 14009−14017.
(22) Lovejoy, E. R.; Hanson, D. R. *J. Phys. Chem.* **1995**, *99*, 2080−2087.
(23) Becker, K. H.; Kleffman, J.; Kurtenbach, R.; Wiesen, P. *J. Phys. Chem.* **1996**, *100*, 14984−14990.
(24) Zhang, R. Y.; Leu, M.-T.; Keyser, L. F. *J. Phys. Chem.* **1996**, *100*, 339−345.
(25) Abbatt, J. P. D.; Nowak, J. B. *J. Phys. Chem. A* **1997**, *101*, 2131−2137.
(26) Robinson, G. N.; Worsnop, D. R.; Jayne, J. T.; Kolb, C. E.; Davidovits, P. *J. Geophys. Res.* **1997**, *102*, 3583−3601.
(27) Hanson, D. R. *J. Phys. Chem. A* **1998**, *102*, 4794−4807.
(28) Horn, A. B.; Sodeau, J. R.; Roddis, T. B.; Williams, N. A. *J. Phys. Chem. A* **1998**, *102*, 6107−6120.
(29) Robinson, G. N.; Worsnop, D. R.; Jayne, J. T.; Kolb, C. E.; Swartz, E.; Davidovitz, P. *J. Geophys. Res.* **1998**, *103*, 25371−25381.
(30) Rudich, Y.; Talukdar, R. K.; Ravishankara, A. R. *J. Geophys. Res.* **1998**, *103*, 16133−16143.
(31) Zhang, Q. L.; Wang, H.; Lana, I. G. D.; Chuang, K. T. *Ind. Eng. Chem. Res.* **1998**, *37*, 1167−1172.
(32) Jayne, J. T.; Worsnop, D. R.; Kolb, C. E.; Swartz, E.; Davidovits, P. *J. Phys. Chem.* **1996**, *100*, 8015−8022.
(33) Middlebrook, A. M.; Iraci, L. T.; McNeil, L. S.; Koehler, B. G.; Wilson, M. A.; Saastad, O. W.; Tolbert, M. A. *J. Geophys. Res.* **1993**, *98*, 20473−20481.
(34) Iraci, L. T.; Tolbert, M. A. *J. Geophys. Res.* **1997**, *102*, 16099−16107.
(35) Guldan, E. D.; Schindler, L. R.; Roberts, J. T. *J. Phys. Chem.* **1995**, *99*, 16059−16066.
(36) Schindler, L. R.; Roberts, J. T. *J. Phys. Chem.* **1996**, *100*, 19582−19586.
(37) Duncan, J. L.; Schindler, L. R.; Roberts, J. T. *Geophys. Res. Lett.* **1998**, *25*, 631−634.
(38) Zhang, R.; Wooldridge, P. J.; Abbatt, J. P. D.; Molina, M. J. *J. Phys. Chem.* **1993**, *97*, 7351−7358.
(39) Massucci, M.; Clegg, S. L.; Brimblecombe, P. *J. Chem. Eng. Data* **1996**, *41*, 765−778.
(40) Tabazadeh, A.; Toon, O. B.; Clegg, S. L.; Hamill, P. *Geophys. Res. Lett.* **1997**, *24*, 1931−1934.
(41) *CRC Handbook of Chemistry and Physics*; 70th ed.; Weast, R. C., Ed.; CRC Publishing: Boca Raton, 1989; pp F-7.
(42) Palmer, K. F.; Williams, D. *Appl. Opt.* **1975**, *14*, 208−219.
(43) Pascard-Billy, C. *Acta Crystallogr.* **1965**, *18*, 827−829.
(44) Steininger, H.; Lehwald, S.; Ibach, H. *Surf. Sci.* **1982**, *123*, 264−270.
(45) Haynes, D. R.; Tro, N. J.; George, S. M. *J. Phys. Chem.* **1992**, *96*, 8502−8509.
(46) King, D. A. *Surf. Sci.* **1972**, *29*, 454−482.
(47) Kubelková, L.; Cejka, J.; Nováková, J. *Zeolites* **1991**, *11*, 48−53.
(48) Banerjee, S. B.; Medhi, K. C. *Ind. J. Phys.* **1960**, *33*, 1−9.
(49) Denbigh, K. G. *The Principles of Chemical Equilibrium*, 4th ed.; Cambridge University Press: New York, 1981.
(50) Williams, L. R.; Long, F. S. *J. Phys. Chem.* **1995**, *99*, 3748−3751.
(51) Williams, L. R. Personal communication.
(52) Steinfeld, J. I.; Francisco, J. S.; Hase, W. L. *Chemical Kinetics and Dynamics*, 2nd ed.; Prentice Hall: Upper Saddle River, 1999.
(53) Liler, M. *Reaction Mechanisms in Sulphuric Acid and Other Strong Acid Solutions*; Academic Press: New York, 1971.
(54) Arnold, F.; Burger, V.; DrosteFanke, B.; Grimm, F.; Krieger, A.; Schneider, J.; Stilp, T. *Geophys. Res. Lett.* **1997**, *24*, 3017−3020.